

Error mitigated variational algorithm on a photonic processor

O.V. Borzenkova^{1,2}, G.I. Struchalin³, I. Kondratyev³, A. Moiseevskiy³, I.V. Dyakonov^{1,3}, and S.S. Straupe^{1,3}

¹*Russian Quantum Center, 30 Bolshoy Boulevard, building 1, Moscow, 121205, Russia*

²*Skolkovo Institute of Science and Technology, 3 Nobel Street, Moscow 121205, Russian Federation and*

³*Quantum Technology Centre and Faculty of Physics, M. V. Lomonosov Moscow State University, 1 Leninskie Gory, Moscow, 119991, Russia*
(*oksana.borzenkova@skoltech.ru)

(Dated: November 27, 2023)

We demonstrate successful error mitigation of indistinguishability-related noise in a quantum photonic processor. We apply zero-noise extrapolation (ZNE) technique to a variational quantum eigensolver (VQE). The observable values measured at two-different error levels allow us to extrapolate it towards noise-free regime. We study influence of the partial distinguishability of photons in a two-qubit processor which implements the VQE for a Schwinger Hamiltonian. The results evidence the improvement of the Hamiltonian eigenvalue estimation using the ZNE procedure. Lastly, we analyze potential applicability of this error mitigation method to other linear optical processors with externally controlled polarization.

I. INTRODUCTION

Noise and errors are still the major obstacles for the development of scalable quantum computers. This problem, at least in theory, is remedied by quantum error correction (QEC). However, QEC requires additional overhead for the most valuable resources — the physical qubits and the circuit depth. The other way around could be careful account of experimentally observable noise processes. In this case the effect of the intrinsic noise in quantum systems can be suppressed for a particular task, for instance, a quantum algorithm implementation. Recently multiple quantum error mitigation (QEM) methods were proposed: zero-noise extrapolation (ZNE) [1, 2], quantum subspace expansion (QSE) [3, 4], purification [5, 6], probabilistic error cancellation (PEC) [7], symmetry verification [8, 9]. Error mitigation may augment the implementation of algorithms on noisy hardware to improve its performance before it reaches the ultimate fault-tolerance threshold.

In the ZNE method, zero-noise value is determined by using data points with different circuit fault rates. QSE technique utilizes a variational subspace spanned by a number of quantum states, which can be generated using additional measurements and post-processing. The target of purification approach is the preparation of an ideal pure state by trying to approximate the pure state closest to real noisy mixed state. The idea of PEC is to express ideal gates as linear combinations called quasi-probability representations of implementable noisy gates and then approximate quantum expectation values. And symmetry verification method is based on identifying errors that break the symmetries of an ideal quantum state and removing them via post-selection. In terms of suitability, all methods can be classified depending on the requirement of a detailed noise model: it is crucial to the last two methods and is not needed for the others. Nonetheless, the purification approach requires additional ancilla qubits, which can be considered a drawback. Experimental demonstrations of the QEM principle include implementation on superconducting processors [7, 10–12] and trapped ion systems [13–15]. While earlier experiments and simulations considered short-depth quantum circuits [7, 16], the more recent research [17] targets the QEM performance on larger-scale de-

vices, which slowly brings the QEM to the realm of the state-of-the-art quantum processors [18–20]. Implementations of QEM on quantum photonic processors are of most relevance for this work. At first the PEC and ZNE methods were put under test to mitigate photon losses in a Gaussian boson sampler [21]. Later the PEC technique was applied as a unified error mitigation scheme for any type of noise [22] and was experimentally demonstrated with a HeH⁺ molecule instance of a VQE algorithm with information encoded in optical ququart states.

A wide range of problems such as quantum metrology [6, 23], solving linear equations [24], quantum Monte Carlo simulation [25], boson sampling [26, 27], and variational simulation [1, 22] benefit from QEM application. We focus on the class of algorithms known as variational quantum eigensolvers (VQE)[28, 29] which find the solution of a problem encoded in a Hamiltonian H by minimizing its average value. The VQE algorithm seeks for the eigenstate corresponding to the minimal eigenvalue of H by minimizing the average values $\langle \psi(\theta) | H | \psi(\theta) \rangle$ measured on the quantum processor for parametrized probe states, where θ denotes the set of parameters which are optimized on a classical computer [30]. The QEM methods were first introduced to quantum computation with short-depth circuits [7] and later adopted to hybrid quantum-classical variational algorithms [11, 22].

In this work, we apply the ZNE mitigation technique to the VQE algorithm which finds the minimal eigenvalue of the Schwinger Hamiltonian on a photonic quantum processor. A key source of errors in photonic architectures is the non-ideal indistinguishability of photons, which affects the Hong-Ou-Mandel (HOM) interference and detrimentally reduces the fidelity of linear-optical two-qubit gates. We demonstrate the power of the ZNE technique by extrapolating data gathered from a photonic processor with controllable indistinguishability towards the noise-free regime.

II. ZERO-NOISE EXTRAPOLATION

Suppose a quantum system is characterized by a *controllable* parameter ε that determines the noise or decoherence strength. We call ε the *noise level*. Let $\varepsilon = 0$ correspond to an

ideal case where all undesirable noise is absent. A common task for ZNE is to estimate an expectation value of some observable $\langle H \rangle$ as if $\varepsilon = 0$, given only a measured data set for $0 < \varepsilon_1 < \dots < \varepsilon_n$:

$$\langle H_{\text{est}}(0) \rangle = F(\langle H(\varepsilon_1) \rangle, \dots, \langle H(\varepsilon_n) \rangle; \varepsilon_1, \dots, \varepsilon_n), \quad (1)$$

where each expectation $\langle H(\varepsilon_k) \rangle$ is the mean of H over noisy states ρ_{noisy} produced by, e. g., a VQE ansatz: $\langle H(\varepsilon_k) \rangle = \text{Tr}(H\rho_{\text{noisy}}(\varepsilon_k))$, $k = 1, \dots, n$. The lowest possible value ε_1 corresponds to intrinsic unavoidable noise in the experimental setup. The approximating function F gives the rule of extrapolation.

Initially, polynomial Richardson approximations were used for ZNE [7], but later exponential approximations proved to be more effective in finding the noise-free value $\langle H(0) \rangle$ [31]. Recent studies [32] introduced adaptive or customised approximations, which can be refined to match a specific problem. A special choice of measured levels $\{\varepsilon_1, \dots, \varepsilon_n\}$ allows to build Richardson extrapolation where estimator's variance does not increase with the polynomial order [2]. Different choices of function types F for approximation are compared in Ref. [33]. Significant theoretical effort is devoted to developing advanced modifications of ZNE [34–37].

In our experiments the noise level ε is related to HOM visibility in the optical chip. As explained in Sec. IV and discussed in [38] the dependence $\langle H(\varepsilon) \rangle$ for $\varepsilon \ll 1$ is well approximated by a linear function:

$$\langle H(\varepsilon) \rangle = c_1 + c_2\varepsilon, \quad (2)$$

where c_1 and c_2 are unknown coefficients. It is sufficient to measure at two points $\varepsilon_{1,2}$ to estimate $c_{1,2}$. Therefore, in our case the general ZNE form (1) reduces to

$$\langle H_{\text{est}}(0) \rangle = \frac{\varepsilon_2 \langle H(\varepsilon_1) \rangle - \varepsilon_1 \langle H(\varepsilon_2) \rangle}{\varepsilon_2 - \varepsilon_1}. \quad (3)$$

It is possible to use more than two points for linear extrapolation [32]. But we stick to the minimal number of points since it is favorable from the experimental point of view — only two expectation values have to be measured so data-acquisition time is significantly reduced.

If the statistical uncertainty σ^2 is the same for each $\langle H(\varepsilon_{1,2}) \rangle$ regardless of $\varepsilon_{1,2}$, the variance of $\langle H_{\text{est}}(0) \rangle$ is

$$\text{var}[\langle H_{\text{est}}(0) \rangle] = \sigma^2 \frac{\varepsilon_2^2 + \varepsilon_1^2}{(\varepsilon_2 - \varepsilon_1)^2}. \quad (4)$$

Note that while the estimate $\langle H_{\text{est}}(0) \rangle$ (3) becomes closer to the noise-free expectation $\langle H(0) \rangle$, its variance (4) may be arbitrarily large as ε_2 approaches ε_1 : $\varepsilon_2 \rightarrow \varepsilon_1$. After error mitigation the average expectation value of a quantum observable becomes more accurate but at the cost of increased standard deviation (see Fig. 1).

III. VARIATIONAL SIMULATION

To verify the efficiency of the mitigation method in experiment, we applied it to a quantum variational algorithm. Theoretical studies of error mitigation in VQA context have been

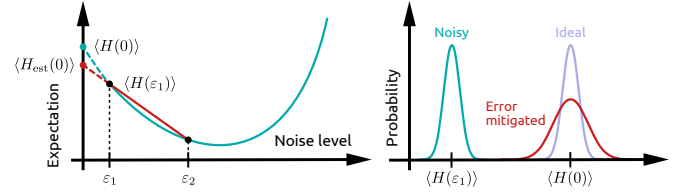


FIG. 1. The idea of zero-noise extrapolation method. Cyan curve describes the dependence of the expected value $\langle H \rangle$ of a Hamiltonian on the noise level ε . The minimal noise level ε_1 is the value closest to an ideal noise-free point which we can obtain experimentally. Red line — extrapolation from two points with different noise levels. The extrapolated result $\langle H_{\text{est}}(0) \rangle$ is closer to $\langle H(0) \rangle$ than the unmitigated result $\langle H(\varepsilon_1) \rangle$.

conducted by the authors of Ref. [39]. In our work, we test the effectiveness of mitigation using a class of VQA called variational quantum eigensolver (VQE) algorithm. The VQE uses a quantum processor to prepare a probe state and measure the expectation value of a Hamiltonian H , which encodes the problem. The probe state is a function of a parameter set, and it can be changed by altering these parameters to minimize the expectation value $\langle H \rangle$. The search over the parameter space is usually a task of a classical optimizer. A good candidate that we have selected is the simultaneous perturbation stochastic approximation (SPSA) algorithm [40]. Since SPSA relates to a class of stochastic approximation methods, it is tolerant to random perturbations in target-function values. This property is important in the experiment because all measured expectations randomly fluctuate around their means due to finite measurement statistics.

We choose the Schwinger model Hamiltonian which was previously studied in the similar setup [41] as a testbed for VQE implementation. For two qubits the Schwinger Hamiltonian has the following form:

$$H_2 = I + \sigma_1^x \sigma_2^x + \sigma_1^y \sigma_2^y - \frac{1}{2} \sigma_1^z + \frac{1}{2} \sigma_1^z \sigma_2^z + \frac{m}{2} (\sigma_2^z - \sigma_1^z), \quad (5)$$

where σ_i ($i = 1, 2$) are the Pauli matrices acting on the qubit i and the parameter m represents the bare mass.

In the experiment the expectation value of a Hamiltonian is measured one term at a time. Then expectations of each Pauli string are added up together on a classical computer. In turn, every Pauli-string expectation is a linear combination of measurement results in a corresponding basis. For example, to measure $\sigma_1^z \sigma_2^z$ one carries out measurements in its eigenbasis $\{|00\rangle, |01\rangle, |10\rangle, |11\rangle\}$, obtaining accumulated outcomes n_{00}, \dots, n_{11} that are proportional to Born-rule probabilities p_{00}, \dots, p_{11} :

$$\langle \sigma_1^z \sigma_2^z \rangle = p_{00} - p_{01} - p_{10} + p_{11} \approx \frac{n_{00} - n_{01} - n_{10} + n_{11}}{n_{00} + n_{01} + n_{10} + n_{11}}. \quad (6)$$

Since the Hamiltonian H_2 can be expressed using three groups of commuting Pauli strings, three bases are enough to measure it completely.

As a result, $\langle H_2 \rangle$ is expressed as a linear combination of

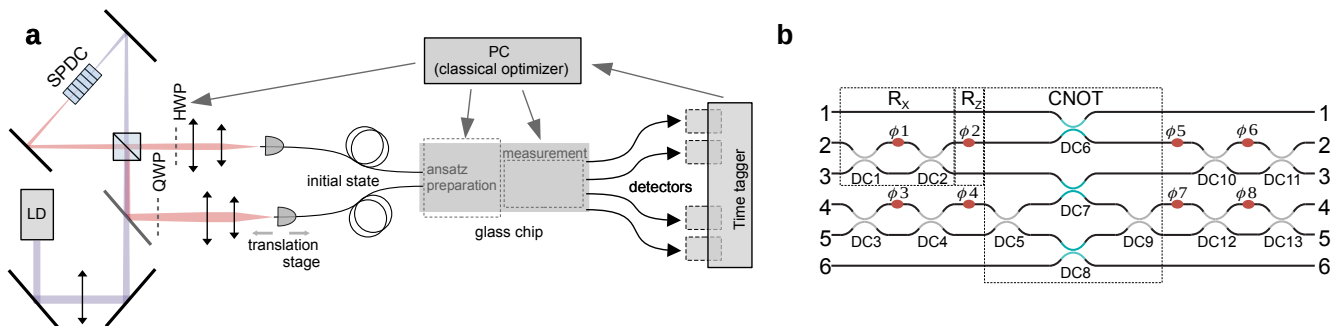


FIG. 2. (a) Experimental setup. Pairs of entangled photons generated in the nonlinear PPKTP crystal are coupled to the input of a programmable glass chip through optical fibers. The fibers at the output of the optical chip are coupled to single-photon superconducting detectors. The detection events are then processed by a time-tagger module and a classical computer. (b) Detailed scheme of the integrated interferometer used in the quantum processor. The interferometer is formed by directional couplers (grey and cyan ones have the splitting ratio of 50:50 and 33:67, respectively) and programmable thermo-optic phase-shifters (red ovals).

outcome probabilities p_k with some real coefficients h_k :

$$\langle H_2 \rangle = \sum_k h_k p_k. \quad (7)$$

Therefore, the dependence $\langle H_2(\varepsilon) \rangle$ on the noise level ε is determined by individual dependencies $p_k(\varepsilon)$.

IV. EXPERIMENTAL SETUP

Performance of linear optical quantum processors is commonly affected by partial distinguishability of photons produced by single photon sources (SPS). The nonlinear-based SPSs indistinguishability is mainly limited by the multiphoton contribution and typically reaches over 99%, Whereas single-emitter based SPSs such as quantum dots, suffer from internal deteriorating processes that are beyond direct control and heavily affect the maximal indistinguishability [42, 43]. In this work we utilize a source of photon pairs based on spontaneous parametric down-conversion (SPDC) and introduce controllable distinguishability by changing the polarization of one photon in a pair relative to the other.

Our two-qubit photonic processor consists of integrated optical interferometer manufactured in SiO_2 by femtosecond laser writing [44]. The photons from SPDC source are injected through polarization-maintaining single-mode optical fibers and outcoupled using regular single-mode fibers connected to superconducting single-photon detectors (see Fig. 2). Photons at the 810 nm wavelength are generated by nonlinear 30-mm PPKTP crystal that is pumped by a 405-nm CW laser diode in the Sagnac configuration. The photon pairs generation rate is 150 kHz.

The elementary blocks of the programmable photonic chip are phase-shifters (PS) and directional couplers (DC), which implement reconfigurable single-qubit gates and a two-qubit CNOT gate (see Fig. 2). The first part of the interferometer (phase-shifters 1-4) prepares the probe state, and the right part (phase-shifters 5-8) sets the measurement basis. The central area of the chip consists of passive DCs, which implement

the probabilistic linear optical CNOT gate with $1/9$ success probability.

A pair of photons generated by the SPDC source is guided to inputs 2 and 4 of the chip to initialize the $|00\rangle$ state in dual-rail encoding. This state is transformed by unitary operations involving two $R_x(\varphi_{1,3})$, two $R_z(\varphi_{2,4})$ gates (one for each qubit), and one CNOT gate. The next step is a projective measurement of each qubit in basis determined by a combination of $R_z(\varphi_{5(7)})$ and $R_x(\varphi_{6(8)})$ gates. We fixed three sets of parameters $\{\varphi_5, \varphi_6, \varphi_7, \varphi_8\}$ to measure the expected value $\langle H \rangle$ in three different bases.

We can verify the indistinguishability of photons produced by the SPDC source by measuring the visibility of a Hong-Ou-Mandel (HOM) interference on a balanced beamsplitter. We observed the best visibility of 98%. In our scheme the depth of HOM dip is affected by three parameters: the photon polarization, wavelength and arrival time. We can adjust the polarization using half- (HWP) and quarter-waveplates (QWP) in different arms of the source. The temperature of the PPKTP crystal controls the wavelengths of the photon pair. We synchronize the photons arrival time by moving a fiber coupler on a linear translation stage in one of the SPDC channels. We first test the source itself using a fiber beamsplitter and as soon as we find the optimal configuration by monitoring the HOM visibility, we connect the source to the chip and test the source parameters by measuring the HOM interference happening directly inside the chip.

By definition we set the noise level $\varepsilon := 1 - V$, where V is the HOM visibility inside the chip. We can measure V by setting the phase φ_4 to π and examining the coincidence counts between outputs 3 and 5. The interference happens at the central directional coupler DC7. The chip has more imperfections than the fiber splitter, and a HOM dip visibility there drops to the value of 82%.

In order to introduce different values of ε , we assume that one photon has a true horizontal polarization $|H\rangle$ and the other is linearly polarized: $\cos(2\theta)|H\rangle + \sin(2\theta)|V\rangle$, where the angle θ can be tuned by inserting a HWP into one arm of the photon source. In our setup the polarization rotation is automated and changing it is the easiest option to control the

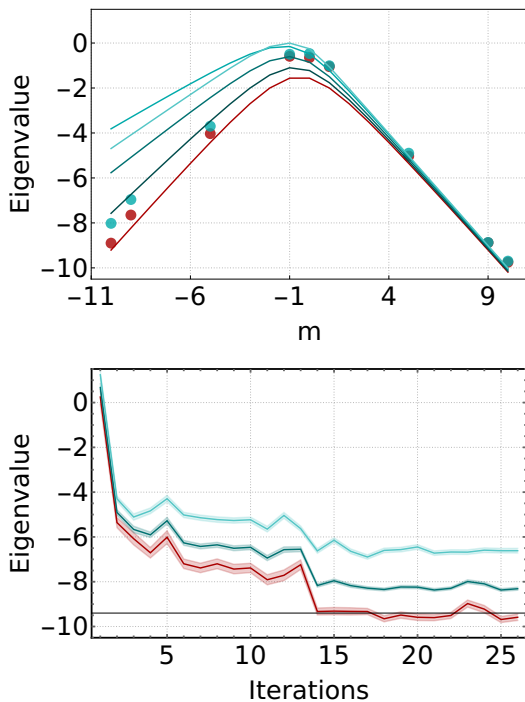


FIG. 3. Top — VQE results for the Schwinger Hamiltonians with different values of m with variable noise level ε : exact eigenvalues (red line), numerical simulations for different values of indistinguishability errors ε (cyan lines), experimental results without and with mitigation (cyan and red dots, respectively). Bottom — optimizer convergence in an experimental run for $m = -10$, cyan curves — experimental results for two different values of indistinguishability $\varepsilon_{1,2}$, red curve — error-mitigated result, filling — one standard deviation of the found eigenvalue under assumption that photon-counting statistics is Poissonian.

degree of indistinguishability.

The functional form of the dependence $\langle H_2 \rangle$ on ε is required for ZNE. In our case, the probabilities of detecting a photon p_k [see Eq. (7)] depend on the HWP rotation angle θ according to Malus law which can be approximated by $p_k \propto \theta^2$ in a vicinity of a minimum. The noise level $\varepsilon = 1 - V$ also depends on the second power of the angle: $\varepsilon \propto \theta^2$, so $p_k \propto \varepsilon$ and, consequently, $\langle H_2 \rangle \propto \varepsilon$. Hence the linear extrapolation model (3) is justified.

We measured visibility V_1 in the case where all adjustable parameters give the highest possible visibility values (an intrinsic noise, ε_1) and V_2 in the case when the half-wave plate is rotated 10 degrees from the optimal position (second noise level ε_2). We found these values to be $V_1 = 82\%$ and $V_2 = 71\%$.

V. RESULTS

A. QEM on a photonic processor

We examined the behavior of the VQE algorithm and compared its convergence with and without error mitigation for

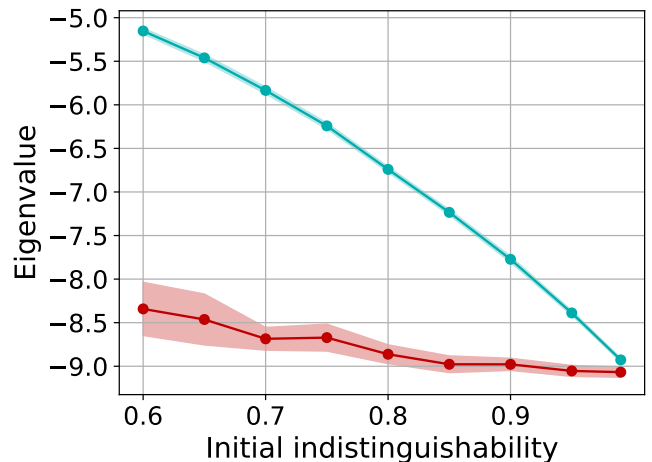


FIG. 4. Eigenvalue dependence on the initial indistinguishability for the Schwinger Hamiltonian H_2 with $m = -10$, cyan curve — simulation without mitigation for different values of indistinguishability (from 60% to 99.9%), red curve — a result of mitigation, where we use two noise levels for approximation: the first level ε_1 is the same as for a cyan curve and the second one is $\varepsilon_2 = t\varepsilon_1$, here ratio $t = 2$ as in experiment, filling — one standard deviation over 100 runs starting from a random initial point.

five different values of the Schwinger Hamiltonian's bare mass parameter m . For each value of m VQE was run without error mitigation and noise level ε_1 . The next step was to test the algorithm with error mitigation — this time, rotating the half-wave plate and making two measurements with different noise levels $\varepsilon_{1,2}$ at each iteration. The obtained zero-noise-extrapolated mean value of the Hamiltonian $\langle H_{\text{est}}(0) \rangle$ is passed to the SPSA optimizer.

Numerical simulations and experimental results show that the convergence of VQE is mostly sensible to noise in the region of negative m , as shown in Fig. 3. We have found that mitigation by ZNE can significantly improve the quality of eigenvalue estimation and obtain the values below the limit set by intrinsic distinguishability of the photon source. These values are closer to the precise eigenvalues. For example, without mitigation the algorithm converges to $E = -7.9 \pm 0.1$ at $m = -10$, while with mitigation we obtain $E = -8.9 \pm 0.6$ (the precise value is $E = -9.2$).

We examined how error mitigation works in the case of different indistinguishability $V = 1 - \varepsilon$ in more detail to assess the method's applicability to large noises. Each point in Fig. 4 is the final eigenvalue found by SPSA after 200 iterations averaged over 100 runs starting from random phases $\{\varphi_1, \dots, \varphi_4\}$. For a relatively poor indistinguishability of 60%, quantum error mitigation allows us to achieve the same results as our processor without error mitigation.

B. Minimizing number of measurements

As we mentioned previously, the strength of the photonic platform is the low level of intrinsic noise, which can be var-

ied externally as part of the mitigation process. However, one of its main drawbacks is the unstable system efficiency during long-term measurements due to temperature and mechanical drifts. Time needed to accumulate sufficient data for one basis measurement depends on the signal intensity. Our SPDC source generated photon pairs at a rate of approximately 150 kHz, but losses and the use of probabilistic CNOT gate caused the signal to drop by two orders of magnitude. With error mitigation, the situation worsens as multiple measurements at different noise levels are required. As a consequence, the experiment becomes time-consuming and, for instance, the accumulated heat within the chip starts to deteriorate the alignment (coupling to the input and output fiber arrays), which further increases the losses and, moreover, makes them asymmetric and time-dependent. To compensate the ongoing drop of photon flux at the chip output during the optimizer run, the signal accumulation at each iteration was performed until a certain number of photons was detected. This ensures constant sample size for every $\langle H_{\text{est}}(0) \rangle$ but at a price of longer data collection time. However, the question of reducing the running time of an algorithm remains relevant.

To partially overcome this problem we propose to turn the mitigation on not from the very beginning but after a certain iteration $k_{\text{mit.}}$ of the optimizer. The value of $k_{\text{mit.}}$ remains unclear but empirical observations indicate that the more iterations the algorithm performs without mitigation, the less time it will take. Experiment time is roughly proportional to the total number of measured bases N needed for estimation of the Hamiltonian expected value. Without mitigation each SPSA iteration uses 6 bases measurements, and when the mitigation is applied this quantity doubles to 12 bases because two noise levels $\epsilon_{1,2}$ must be accounted.

We conducted numerical simulations of the experiment where we examined the dependence of relative error $A(N, k_{\text{mit.}})$ for the considered algorithm on the iteration at which the mitigation is activated $k_{\text{mit.}}$ and tracked the number N of measured bases (actually, N is recalculated from the number of SPSA iterations). Relative error $A(N, k_{\text{mit.}})$ is defined as follows:

$$A(N, k_{\text{mit.}}) = \frac{E(N, k_{\text{mit.}}) - E_0}{E(N, 0) - E_0}, \quad (8)$$

where $E(N, k_{\text{mit.}})$ is the Hamiltonian eigenvalue found by the VQE algorithm utilizing N measurements in total with mitigation applied since iteration $k_{\text{mit.}}$, and E_0 is the exact ground energy. Obviously, when mitigation is turned on from the very beginning the relative error is equal to unity: $A(N, 0) = 1$.

During a VQE run, mitigation can be turned on in two different scenarios. The first one simply begins to feed mitigated values to the optimizer. This is equivalent to a sudden substitution of the optimized function. The second one restarts the optimizer from scratch when mitigation is switched on, using the latest probe state configuration as the initial guess. A deliberate examination of both options evidenced that the second approach ends up with a higher accuracy A of expected value estimation.

Simulations were run with the same visibility, parameters of the classical SPSA optimizer, and other variables as in the

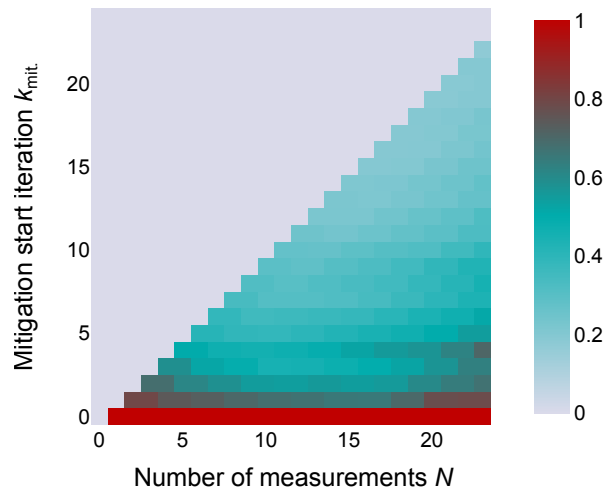


FIG. 5. Simulation of a hybrid approach. Mitigation is triggered at an iteration $k_{\text{mit.}}$ indicated by the y-axis, while number of measurements N is shown by the x-axis. The color scale indicates the algorithm relative error $A(N, k_{\text{mit.}})$ (see text for explanation) where found eigenvalues are averaged over 100 runs.

experiment. We test the algorithm without mitigation starting from different initial points and activating mitigation at a specified iteration $k_{\text{mit.}}$. Based on averaging over the resulting Hamiltonian eigenvalues, we calculate the relative error A (8) for various $k_{\text{mit.}}$ and the number of measured bases N . The results are shown in Fig. 5. For the same N the error A does not increase with the growth of $k_{\text{mit.}}$ and, mainly, the best precision is achieved when mitigation is postponed till the end: $k_{\text{mit.}} \approx N$. Therefore, the experiment duration can be reduced compared to the case when mitigation is always on ($k_{\text{mit.}} = 0$) without sacrificing the accuracy of the eigenvalue estimation.

VI. CONCLUSION

We have experimentally demonstrated zero-noise extrapolation method to mitigate the errors in linear-optical quantum processor caused by partial distinguishability of photons. The method is experimentally friendly, easy to implement, and may be used for any linear-optical processors with dual-rail encoded qubits where the calibrated indistinguishability control knob is present. We found that linear extrapolation using two values of indistinguishability is a simple and efficient method. We have experimentally studied the performance of the proposed method in the case of a VQE algorithm for the two-qubit Schwinger model Hamiltonian and found that error-mitigated algorithm is capable of estimating the eigenvalues with precision beyond the limitations introduced by intrinsic distinguishability of the photon source. We expect that such mitigation strategy may be widely adopted in linear-optical quantum computing in order to overcome the burden of non-ideal indistinguishability observed in the state-of-the-art efficient single-photon sources [43].

ACKNOWLEDGMENTS

The authors acknowledge support by Rosatom in the framework of the Roadmap for Quantum computing (Contract

No. 868-1.3-15/15-2021 dated October 5, 2021 and Contract No.P2154 dated November 24, 2021). I.D. acknowledges support from Russian Science Foundation grant 22-12-00353 (<https://rscf.ru/en/project/22-12-00353/>).

-
- [1] Y. Li and S. C. Benjamin, Efficient variational quantum simulator incorporating active error minimization, *Physical Review X* **7**, 021050 (2017).
- [2] M. Krebsbach, B. Trauzettel, and A. Calzona, Optimization of richardson extrapolation for quantum error mitigation, *Physical Review A* **106**, 062436 (2022).
- [3] J. R. McClean, M. E. Kimchi-Schwartz, J. Carter, and W. A. De Jong, Hybrid quantum-classical hierarchy for mitigation of decoherence and determination of excited states, *Physical Review A* **95**, 042308 (2017).
- [4] J. R. McClean, Z. Jiang, N. C. Rubin, R. Babbush, and H. Neven, Decoding quantum errors with subspace expansions, *Nature communications* **11**, 636 (2020).
- [5] T. E. O'Brien, G. Anselmetti, F. Gkritis, V. Elfving, S. Polla, W. J. Huggins, O. Oumarou, K. Kechedzhi, D. Abanin, R. Acharya, *et al.*, Purification-based quantum error mitigation of pair-correlated electron simulations, arXiv preprint arXiv:2210.10799 (2022).
- [6] K. Yamamoto, S. Endo, H. Hakoshima, Y. Matsuzaki, and Y. Tokunaga, Error-mitigated quantum metrology via virtual purification, *Physical Review Letters* **129**, 250503 (2022).
- [7] K. Temme, S. Bravyi, and J. M. Gambetta, Error mitigation for short-depth quantum circuits, *Physical review letters* **119**, 180509 (2017).
- [8] S. McArdle, X. Yuan, and S. Benjamin, Error-mitigated digital quantum simulation, *Physical review letters* **122**, 180501 (2019).
- [9] X. Bonet-Monroig, R. Sagastizabal, M. Singh, and T. O'Brien, Low-cost error mitigation by symmetry verification, *Physical Review A* **98**, 062339 (2018).
- [10] A. Kandala, K. Temme, A. D. Córcoles, A. Mezzacapo, J. M. Chow, and J. M. Gambetta, Error mitigation extends the computational reach of a noisy quantum processor, *Nature* **567**, 491 (2019).
- [11] R. Sagastizabal, X. Bonet-Monroig, M. Singh, M. A. Rol, C. C. Bultink, X. Fu, C. H. Price, V. P. Ostroukh, N. Muthusubramanian, A. Bruno, M. Beekman, N. Haider, T. E. O'Brien, and L. DiCarlo, Experimental error mitigation via symmetry verification in a variational quantum eigensolver, *Phys. Rev. A* **100**, 010302 (2019).
- [12] S. Bravyi, S. Sheldon, A. Kandala, D. C. McKay, and J. M. Gambetta, Mitigating measurement errors in multiqubit experiments, *Phys. Rev. A* **103**, 042605 (2021).
- [13] S. Zhang, Y. Lu, K. Zhang, W. Chen, Y. Li, J.-N. Zhang, and K. Kim, Error-mitigated quantum gates exceeding physical fidelities in a trapped-ion system, *Nature communications* **11**, 587 (2020).
- [14] O. G. Maupin, A. D. Burch, C. G. Yale, B. Ruzic, A. Russo, D. S. Lobser, M. C. Revelle, M. N. Chow, S. M. Clark, A. J. Landahl, *et al.*, Error mitigation, optimization, and extrapolation on a trapped ion testbed, arXiv preprint arXiv:2307.07027 (2023).
- [15] W. Chen, S. Zhang, J. Zhang, X. Su, Y. Lu, K. Zhang, M. Qiao, Y. Li, J.-N. Zhang, and K. Kim, Error-mitigated quantum simulation of interacting fermions with trapped ions, arXiv preprint arXiv:2302.10436 (2023).
- [16] S. Ferracin, A. Hashim, J.-L. Ville, R. Naik, A. Carignan-Dugas, H. Qassim, A. Morvan, D. I. Santiago, I. Siddiqi, and J. J. Wallman, Efficiently improving the performance of noisy quantum computers, arXiv preprint arXiv:2201.10672 (2022).
- [17] Y. Kim, C. J. Wood, T. J. Yoder, S. T. Merkel, J. M. Gambetta, K. Temme, and A. Kandala, Scalable error mitigation for noisy quantum circuits produces competitive expectation values, *Nature Physics* , 1 (2023).
- [18] E. J. Zhang, S. Srinivasan, N. Sundaresan, D. F. Bogorin, Y. Martin, J. B. Hertzberg, J. Timmerwilke, E. J. Pritchett, J.-B. Yau, C. Wang, *et al.*, High-performance superconducting quantum processors via laser annealing of transmon qubits, *Science Advances* **8**, eabi6690 (2022).
- [19] F. Arute, K. Arya, R. Babbush, D. Bacon, J. C. Bardin, R. Barends, R. Biswas, S. Boixo, F. G. Brandao, D. A. Buell, *et al.*, Quantum supremacy using a programmable superconducting processor, *Nature* **574**, 505 (2019).
- [20] Y. Wu, W.-S. Bao, S. Cao, F. Chen, M.-C. Chen, X. Chen, T.-H. Chung, H. Deng, Y. Du, D. Fan, *et al.*, Strong quantum computational advantage using a superconducting quantum processor, *Physical review letters* **127**, 180501 (2021).
- [21] D. Su, R. Israel, K. Sharma, H. Qi, I. Dhand, and K. Brádler, Error mitigation on a near-term quantum photonic device, arXiv preprint arXiv:2008.06670 (2020).
- [22] D. Lee, J. Lee, S. Hong, H.-T. Lim, Y.-W. Cho, S.-W. Han, H. Shin, J. ur Rehman, and Y.-S. Kim, Error-mitigated photonic variational quantum eigensolver using a single-photon ququart, *Optica* **9**, 88 (2022).
- [23] L. O. Conlon, T. Vogl, C. D. Marciniak, I. Pogorelov, S. K. Yung, F. Eilenberger, D. W. Berry, F. S. Santana, R. Blatt, T. Monz, *et al.*, Approaching optimal entangling collective measurements on quantum computing platforms, *Nature Physics* **19**, 351 (2023).
- [24] A. C. Vazquez, R. Hiptmair, and S. Woerner, Enhancing the quantum linear systems algorithm using richardson extrapolation, *ACM Transactions on Quantum Computing* **3**, 1 (2022).
- [25] Y. Yang, B.-N. Lu, and Y. Li, Accelerated quantum monte carlo with mitigated error on noisy quantum computer, *PRX Quantum* **2**, 040361 (2021).
- [26] S. Endo, Y. Suzuki, K. Tsubouchi, R. Asaoka, K. Yamamoto, Y. Matsuzaki, and Y. Tokunaga, Quantum error mitigation for rotation symmetric bosonic codes with symmetry expansion, arXiv preprint arXiv:2211.06164 (2022).
- [27] M. Tillmann, B. Dakić, R. Heilmann, S. Nolte, A. Szameit, and P. Walther, Experimental boson sampling, *Nature Photonics* **7**, 540 (2013).
- [28] A. Peruzzo, J. McClean, P. Shadbolt, M.-H. Yung, X.-Q. Zhou, P. J. Love, A. Aspuru-Guzik, and J. L. O'Brien, A variational eigenvalue solver on a photonic quantum processor, *Nature communications* **5**, 4213 (2014).
- [29] J. Tilly, H. Chen, S. Cao, D. Picozzi, K. Setia, Y. Li, E. Grant, L. Wossnig, I. Rungger, G. H. Booth, *et al.*, The variational quantum eigensolver: a review of methods and best practices, *Physics Reports* **986**, 1 (2022).

- [30] M. Cerezo, A. Arrasmith, R. Babbush, S. C. Benjamin, S. Endo, K. Fujii, J. R. McClean, K. Mitarai, X. Yuan, L. Cincio, *et al.*, Variational quantum algorithms, *Nature Reviews Physics* **3**, 625 (2021).
- [31] S. Endo, S. C. Benjamin, and Y. Li, Practical quantum error mitigation for near-future applications, *Physical Review X* **8**, 031027 (2018).
- [32] T. Giurgica-Tiron, Y. Hindy, R. LaRose, A. Mari, and W. J. Zeng, Digital zero noise extrapolation for quantum error mitigation, in *2020 IEEE International Conference on Quantum Computing and Engineering (QCE)* (IEEE, 2020) pp. 306–316.
- [33] T. Giurgica-Tiron, Y. Hindy, R. LaRose, A. Mari, and W. J. Zeng, Digital zero noise extrapolation for quantum error mitigation, in *2020 IEEE International Conference on Quantum Computing and Engineering (QCE)* (2020) pp. 306–316.
- [34] A. Lowe, M. H. Gordon, P. Czarnik, A. Arrasmith, P. J. Coles, and L. Cincio, Unified approach to data-driven quantum error mitigation, *Physical Review Research* **3**, 033098 (2021).
- [35] Z. Cai, Multi-exponential error extrapolation and combining error mitigation techniques for nisq applications, *npj Quantum Information* **7**, 80 (2021).
- [36] V. R. Pascuzzi, A. He, C. W. Bauer, W. A. De Jong, and B. Nachman, Computationally efficient zero-noise extrapolation for quantum-gate-error mitigation, *Physical Review A* **105**, 042406 (2022).
- [37] A. He, B. Nachman, W. A. de Jong, and C. W. Bauer, Zero-noise extrapolation for quantum-gate error mitigation with identity insertions, *Physical Review A* **102**, 012426 (2020).
- [38] C. Dittel, G. Dufour, G. Weihs, and A. Buchleitner, Wave-particle duality of many-body quantum states, *Physical Review X* **11**, 031041 (2021).
- [39] G. S. Barron and C. J. Wood, Measurement error mitigation for variational quantum algorithms, arXiv preprint arXiv:2010.08520 (2020).
- [40] S. Bhatnagar, H. Prasad, and L. Prashanth, *Stochastic Recursive Algorithms for Optimization*, 1st ed. (Springer London) p. 302.
- [41] O. V. Borzenkova, G. I. Struchalin, A. S. Kardashin, V. V. Krasnikov, N. N. Skryabin, S. S. Straupe, S. P. Kulik, and J. D. Biamonte, Variational simulation of Schwinger’s Hamiltonian with polarization qubits, *Applied Physics Letters* **118**, 144002 (2021), https://pubs.aip.org/aip/apl/article-pdf/doi/10.1063/5.0043322/14547816/144002_1_online.pdf.
- [42] M. Rakhlin, A. Galimov, I. Dyakonov, N. Skryabin, G. Klimko, M. Kulagina, Y. M. Zadiranov, S. Sorokin, I. Sedova, Y. A. Guseva, *et al.*, Demultiplexed single-photon source with a quantum dot coupled to microresonator, *Journal of Luminescence* **253**, 119496 (2023).
- [43] N. Tomm, A. Javadi, N. O. Antoniadis, D. Najer, M. C. Löbl, A. R. Korsch, R. Schott, S. R. Valentin, A. D. Wieck, A. Ludwig, *et al.*, A bright and fast source of coherent single photons, *Nature Nanotechnology* **16**, 399 (2021).
- [44] N. Skryabin, I. Kondratyev, I. Dyakonov, O. Borzenkova, S. Kulik, and S. Straupe, Two-qubit quantum photonic processor manufactured by femtosecond laser writing, *Applied Physics Letters* **122** (2023).